Unraveling Atomic and Electronic Surface Structure and Dynamics from Angular Photoelectron Distributions

Matthias Hengsberger[a]*, Luca Castiglioni[a], and Jürg Osterwalder[a]

Abstract: Angle-resolved photoelectron spectroscopy (ARPES) is a powerful tool in solid state sciences. Beside the direct measurement of the energy-momentum dispersion relation, the angular distribution of the photoelectron current reveals the structural environment of the emitting atoms via photoelectron diffraction effects. Moreover, in the case of molecular layers, the angular distribution of emission from molecular orbitals can be directly related to their charge density distribution via so-called orbital tomography. In the present paper we summarize our efforts undertaken over the past 12 years to add the dimension of time to these two methods via pump-probe experiments with femtosecond resolution. We give a comprehensive introduction to standard ARPES and time-resolvedtwo-photon photoemission and then focus on our efforts towards time-resolved versions of photoelectron diffraction and orbital tomography. Both, optimization of experimental parameters and data acquisition procedures, as well as new numerical tools are needed in order to realize such challenging full stop missing after experiments.

Keywords: Electron and structural dynamics · Solid-molecule interfaces · Photoemission · Photoelectron Diffraction · Ultrafast Pump-Probe Spectroscopy

Matthias Hengsberger studied physics at the Universität des Saarlandes (Saarbrücken, Germany). He obtained his Ph.D. from the Université de Neuchâtel working in the group of Y. Baer on the signature of many-body interactions in photoelectron spectra. He then joined the group of J. Osterwalder at the Universität Zürich. His research interests are photoelectron spectroscopy including band structure analysis, many-body physics, and ultrafast dynamics, in particular in metallic and semi-conducting solids.

Luca Castiglioni studied chemistry at ETH Zürich, where he also obtained his Ph.D. in physical chemistry in the group of P. Chen working on photodissociation and excited state dynamics. After a postdoctoral stay at UC Berkeley in the group of D. Neumark, he spent a year with the Molecular Dynamics Group at PSI Villigen. In 2011 he joined the group of J. Osterwalder at UZH as senior scientist. His research at UZH focuses on interfacial electron dynamics, in particular molecular layers on semi-conducting substrates, studied by time-resolved photoemission and orbital tomography.

Jürg Osterwalder studied physics at ETH Zürich and graduated in the group of H.C. Siegmann in 1985. During a postdoctoral stay in the group of C. Fadley at the University of Hawaii, he became familiar with photoelectron diffraction, which he helped to establish as an important tool in surface science after joining the group of L. Schlapbach at the Université de Fribourg.

Since 1994 he is professor at the Physics Department at UZH. His research covers many topics in surface science ranging from metalsemiconductor interfaces over topological materials to heterogeneous catalysis.

Introduction: Photoemission from Surfaces

God made the bulk, the surface was invented by the Devil. This famous sentence is attributed to Wolfgang Pauli[1] who thereby expressed the embarrassment of having to deal with a discontinuity in an otherwise perfectly periodic lattice. The surface atoms have different environment due to missing chemical bonds at the outer surface. Therefore, the electronic charge distribution and the atomic positions adapt in order to minimize the surface free energy. The surface properties are the key for charge transfer at interfaces between solids or solids and their gaseous or liquid environment, and their understanding is thus crucial for any application in *e.g.* catalytic processes. Moreover, the surface properties can be tuned by deposition of thin solid films or molecular layers in order to enhance electron transfer rates and, thereby, catalytic activity, or else protect unstable material against corrosion in harsh environments, for instance.[2]

For the investigation of the electronic and atomic structure of surface systems, a full wealth of methods are available, like scanning probe microscopies, electron diffraction or photoelectron spectroscopy. While most experiments are taking place in ultrahigh vacuum under well defined conditions in order to avoid contamination of the surfaces by residual gases, special techniques and setups allow measurements in ambient pressure[4] or even in liquid environments.[5]

In the present paper we will give an overview of recent developments in photoelectron spectroscopy from ordered surface systems with special emphasis on experiments to observe electron and structural dynamics on femtosecond timescales in systems excited by light. After a short general introduction to angle-resolved photoemission, the results of one of our own time-resolved studies will be presented in order to highlight the power of fem-

Correspondence: [a]Department of Physics, University of Zurich, Winterthurerstrasse 190, CH-8057 Zürich, Switzerland, e-mail: matthias.hengsberger@physik.uzh.ch

tosecond pump-probe photoemission measurements and the need for advanced theory tools to understand and interpret such data. In the subsequent section, two effects contributing to the angular distribution and the interpretation of the resulting patterns will be reviewed: (i) the scattering of the photoelectrons at neighboring atoms (photoelectron diffraction) and (ii) the anisotropic emission due to the initial state wavefunction (orbital tomography). We discuss the experimental realization and information. We wish to point out that this paper is not meant to provide a comprehensive review over these fields but to highlight the additional feasibility studies carried out by us in the framework of a Swiss National Center of Competence in Research in order to extend the scope of conventional spectroscopies into the femtosecond time domain. At the end of this paper and as an outlook, we will conclude by giving an overview over the current possibilities to carry out experiments at user facilities.
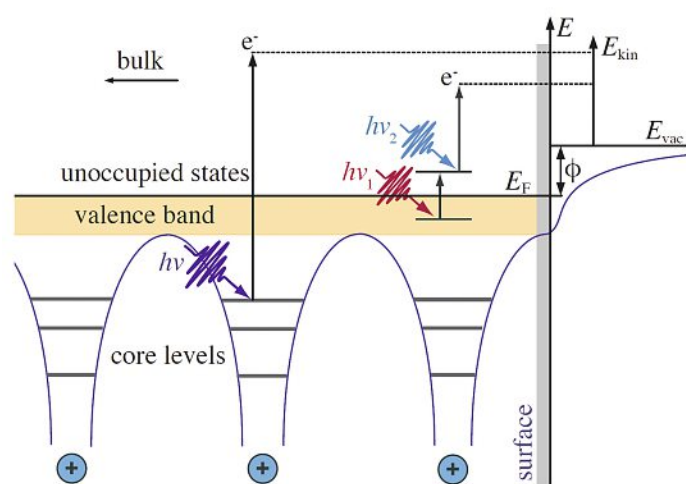

Fig. 1: Scheme of the photoemission process: an electron makes an optical transition out of a core or valence state after absorption of a photon of energy $h\nu$ into a free-electron-like final state. If the final state energy is larger than the vacuum energy E_{vac} the electron can be emitted to the vacuum where it is detected as function of its kinetic energy E_{kin}. Using a two-photon sequence one may transiently populate un unoccupied state by $h\nu_1$ (pump) and use a second photon $h\nu_2$ to probe this transient state. (Adapted from Ref. 3.)

Angle-resolved Photoelectron Spectroscopy (ARPES)

Angle-resolved photoelectron spectroscopy (ARPES) is a widely used tool in solid state sciences to access the momentum-resolved electronic structure of solids. A comprehensive overview can be found in many reviews and books, like *e.g.* the book of Hüfner.[6] Briefly, the method is based on the photoelectric effect: Absorption of a vacuum ultraviolet photon (VUV, 8-50 eV, with extended range up to ≈100 eV, termed EUV or XUV) or soft x-ray photon (above VUV up to 1 keV) leads to the emission of a photoelectron. By measuring the kinetic energy of the photoelectron and using energy conservation the binding energy of the electron in the solid can be calculated and referenced to some particular energy level like the Fermi E_F. Depending on the range of photon energies used, one speaks of ultraviolet photoelectron spectroscopy (UPS) or x-ray photoelectron spectroscopy (XPS). In ARPES, the emission angle of the photoelectron from a single-crystalline sample is measured in addition to its kinetic energy. From this we can calculate the momentum vector inside the crystal as follows: Due to the translational symmetry of the crystal surface parallel and the broken symmetry of the truncated crystal perpendicular to the surface plane, the parallel component of the momentum of the photoelectron is conserved in the emission pro-

cess. The component perpendicular to the surface plane is not conserved due to the broken symmetry of the truncated crystal perpendicular to the surface plane. In the so-called free-electron final state approximation the photoelectron is described as a plane wave propagating inside the crystal in a constant potential V0, the inner potential. The value of V_0 is usually obtained by fitting and of the order of 10 eV.[6] At the surface the potential rises to the vacuum level, which reduces the kinetic energy of the photoelectron. This can be treated like an optical refraction using Snell's law. Finally, we can determine the electron momentum inside the solid and, together with the binding energy of the initial state, the full dispersion relation $E(\vec{k}) - E_F$:

$$
\begin{aligned}
E(\vec{k}) - E_F &= E_{\mathrm{kin}} - (h\nu - \phi) \\
k_\perp &= \sqrt{\frac{2m}{\hbar^2}\left(E_{\mathrm{kin}}\cos^2\theta - V_0\right)} \\
k_\| &= \sqrt{\frac{2m}{\hbar^2}E_{\mathrm{kin}}}\sin\theta = 0.512\,\text{Å}^{-1}\sqrt{\frac{E_{\mathrm{kin}}}{1\,\text{eV}}}\sin\theta
\end{aligned} \tag{1}
$$

Here $h\nu$, φ, θ, and E_{kin} denote the photon energy, the work-function of the sample surface, the polar emission angle with respect to the surface normal, and the kinetic energy measured in vacuum, respectively. $k_\|$ and $k_\perp$ are the wavevector components inside the crystal and parallel and perpendicular to the sample surface, respectively, which are related to the crystal momentum vector by $\vec{p} = \hbar\vec{k}$. In the case of two-dimensional (2D) systems like monolayers of organic molecules, there is no dispersion with component perpendicular to the surface, and the relevant component parallel to the surface can be calculated using momentum conservation according to Eqn. 1. Owing to the periodic crystal structure, the momentum, however, is only conserved modulo a reciprocal lattice vector, which means that we may expect contributions from higher Brillouin zones in our ARPES spectra. In practice these contributions have very weak intensities as demonstrated by Voit and co-workers.[7] Therefore, we may assume that the free-electron-like final state in the surface has the same parallel component of the momentum as the free photoelectron in vacuum. The mean-free path of electrons in the final state is very small, ranging from a few Ångström at kinetic energies of about 50 eV to roughly 1 nm at 1 keV. The mean-free path follows for most materials the so-called universal curve which has a minimum around 50 eV and increases with the square root of the energy towards higher energy.[6] From this curve one might expect a large mean-free path when going from the minimum towards low energy[8] but even at typical laser photon energies of about 6 eV ARPES the probing depth is limited to about 1 nm according to experience. There is a second effect of the limited mean-free path $\Lambda(E_{\mathrm{kin}})$, which should be kept in mind: the exponential decay of a free-electron-like wave translates into a broadened perpendicular component of the electron momentum of the order of $\Delta k_\perp \approx \Lambda(E_{\mathrm{kin}})^{-1}$. This means that in case of truly 3D material, the momentum resolution can be greatly enhanced increasing the energy, and thereby $\Lambda(E_{\mathrm{kin}})$. Thus, for practical purposes, the experimental parameters will always be a compromise between the accessible range versus resolution in energy and momentum[8], photoionization cross-sections[9], and finally the stability of the sample, which often limits the time available for the measurements.

Besides the bare dispersion relation and many-body effects, the treatment of which is beyond the scope of this paper, the angular distribution of the photocurrent contains a lot of additional valuable information which can be exploited to obtain information about the equilibrium and transient atomic structure and electronic density distribution as we will see below.

Time-resolved ARPES

Our goal is not to give a full account of time-resolved photoemission here but simply to demonstrate, using the results of a recent project as an example, how the concept works and how it can be used as a platform for extending related methods to the time domain. As schematically shown in Fig. 1, photoelectrons can not only be generated by single photons of sufficient energy but also using a sequence of two photons in separate light pulses: the first pulse populates an intermediate state (pump pulse) and the second pulse then probes the transient population (probe pulse). The method is then called two photon photoemission (2PPE). By varying the time delay between pump and probe pulses the dynamics like *e.g.* population relaxation rates can be measured in real time and with femtosecond resolution (see *e.g.* Ref. 10 for a review). For such purposes, low photon energies between about 3 and 6 eV are often used, the sum of which must be sufficient to excite the electrons above the vacuum level. Such pulses can conveniently be produced using non-linear optical crystals and the output of a commercial femtosecond laser system, which usually provides near-infrared pulses of 800 to 1064 nm (1.55 to 1.17 eV).
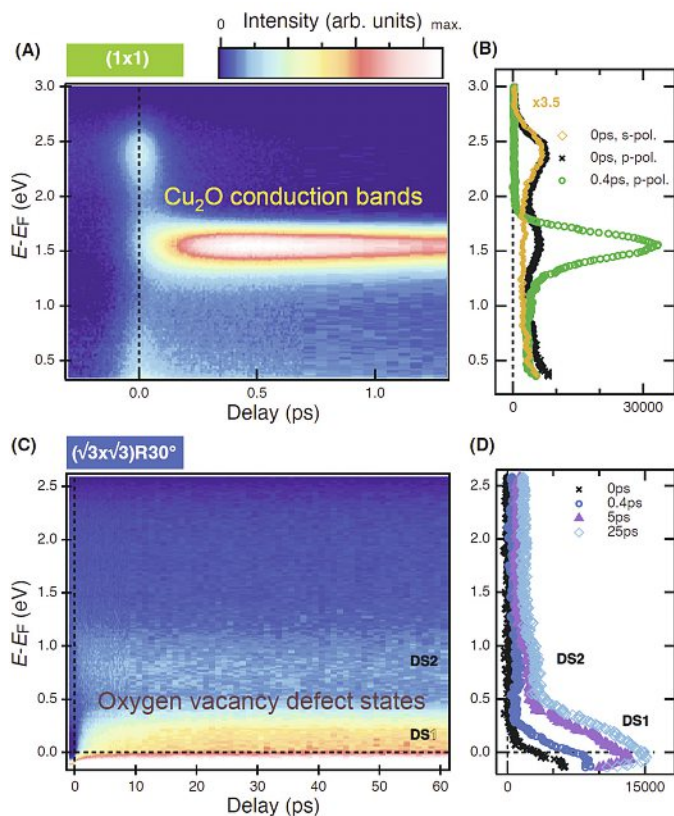
The dynamics and energy distributions of the electrons reaching the surface are very different in the two cases. The surface producing a (1 x 1) low-energy electron diffraction (LEED) pattern, suggesting a surface-truncated bulk-like structure, shows population of two conduction band states at the surface [Fig. 2(A) and (B)]. The one at higher energy (CBS at 2.4 eV) decays on a time scale of a few tens of femtoseconds, while the one at lower energy represents the conduction band minimum (CBM at 1.5 eV) that decays over a longer time scale. Using such data sets we can extract the intensity of the states as function of delay as shown in Fig. 3 for the Cu_2O data. The transient intensity is directly proportional to the intermediate state population and is often analyzed using rate equations in order to obtain the time constants and excited state lifetimes. This analysis leads to lifetime values $\tau = 30$ fs for the CBS and 10 ps for the CBM [Fig. 3(A) and (B)].
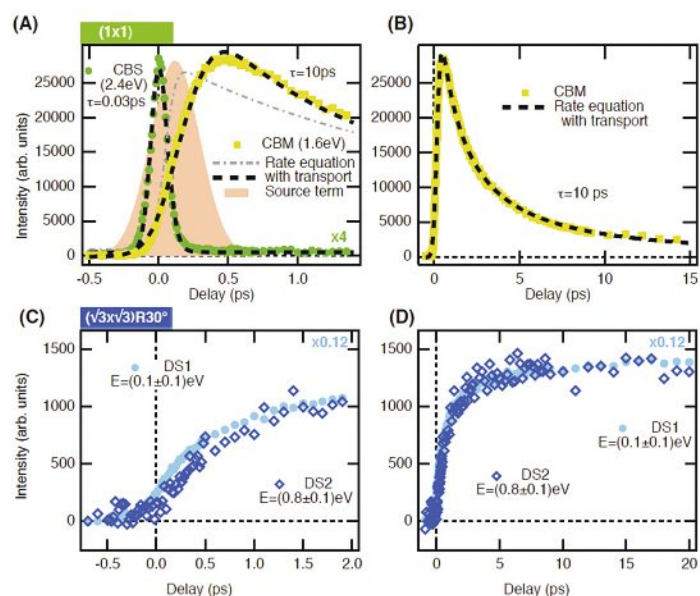

Fig. 3: Transient populations of the excited states extracted from the data sets shown in Fig. 2. The curves are asymmetric with a sharp rise near coincidence of the two pulses and exponential decay towards positive delays, i.e. when the pump pulse precedes the probe pulse. The time constant obtained by fitting a model function to the intensity measured at the conduction band minimum CBM is given in the plot (B). (Taken from ref. 11.)

Fig. 2: Time-resolved 2PPE from Cu_2O(111) using 3 eV pump and 6 eV probe pulses: The false-color plots (A) and represent the photoemission intensity in normal emission as function of energy (vertical axis) and pump-probe time delay (horizontal axis) for (A) the stoichiometric 1×1-surface and (C) an oxygen-deficient $\sqrt{3} \times \sqrt{3}$ R30°-surface. (B) and show spectra extracted for selected time delays. (Adapted from ref. 11.)

As an example to highlight the power of time-resolved ARPES, data are shown in Fig. 2 which were taken from cuprous oxide Cu_2O for two different surface treatments, the preparation of a bulk-terminated, stoichiometric 1x1-surface and a second preparation which produces a surface layer with a high density of oxygen vacancies. The latter vacancies mutually repel each other and form an ordered surface reconstruction with a $\sqrt{3} \times \sqrt{3}$ R30° periodicity.[11]

For the oxygen deficient surface showing a ($\sqrt{3} \times \sqrt{3}$) R30° periodicity according to LEED measurements, the conduction bands are completely suppressed [2(C) and (D)] which means that the electrons excited into the conduction band over the light absorption length of about 30 nm do not reach the surface but are trapped in low energy states caused by defects. The transients displayed in Fig. 3(C) and (D) show that the populations of two trap states (DS1 and DS2) at the surface build up gradually over a time scale of about 1 ps and that their relaxation times are very long, exceeding the delay times that can be reached with a movable delay stage in such femtosecond time-resolved 2PPE experiments.

The charge distribution, energy levels, and concomitant lattice deformations of such defects can be modeled using density-functional theory (DFT) in supercell slab geometries for different charge states of the vacancies.[12] Comparing time-resolved spectra of the defect states with the DFT results then allows us to identify the charge states and compute the capture coefficients. The charge distributions of the trapped states and the suggested trapping processes modeled in these calculations are visualized in Fig. 4. Since the oxygen defects in the ($\sqrt{3} \times \sqrt{3}$)R30° surface
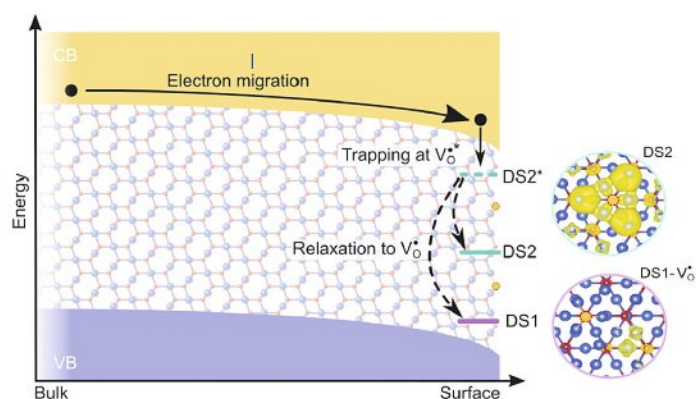
Fig. 4: Model calculation for the trapping of excited electrons by singly-charged oxygen vacancies: electrons excited in the bulk are driven to the surface by the surface depletion layer in Cu_2O. Using certain preparation conditions, a high density of oxygen vacancies is generated in the surface The charge distribution of the two defect states is plotted on the right- hand-side. (Adapted from ref. 12.)

Fig. 5: Scheme of a typical photoemission experiment: in most cases the geometry of light sources and analyzer axis (here named **k**) is fixed. The sample is rotated around two axes, and the polar angle and the sample azimuth are varied. A pattern is recorded by sequential rotation and data acquisition steps[14]. Bottom panel: elastic scattering probability as function of scattering angle for two kinetic energies, 25 eV (black dashed line) and 772 eV (red line). (Taken from ref. 15.)

are situated mainly in the top surface layer, these experiments furthermore illustrate the high surface sensitivity of 2PPE at these photon energies.

We emphasize here that such investigations are beyond the possibilities of conventional ARPES studies because the relevant states are only transiently populated and thus invisible for one-photon-photoemission experiments.

As already mentioned in the preceding section, the use of low photon energies has certain advantages like high cross-sections and increased momentum resolution. In many cases, however, the important dynamics take place at higher momenta, like *e.g.* at the border of the Brillouin zone. The momentum range accessible to the experiment is essentially given by the photon energy (see Eqn. 1): To reach sufficiently large momenta to cover the full Brillouin zone the photon energy must by increased. As a rule of thumb, photon energies of the order of 20 eV are used in ARPES from fcc metals like Cu or Au to reach the high symmetry points at $k \approx 1.5$ Å^{-1}.[6] Femtosecond pulses with VUV photon energies for ARPES can be produced in laboratory scale experiments using high-harmonic generation (HHG)[13] as will briefly be discussed in the final section of this paper.

Photoelectron Diffraction

The geometry of a typical angle-resolved photoemission experiment is sketched in Fig. 5. One way of recording the full emission pattern is to vary the sample orientation with respect to the electron detection direction and to record spectra or photoelectron intensities at each step.[14] It was realized early on that the intensity of core level photoelectrons exhibits maxima which are caused by elastic scattering of the photoelectrons at neighboring atoms of the emitter atom.[16] The direct wave and the scattered waves interfere and produce a pattern in the far field, similar to an holographic image of the emitter environment.[17] Moreover, at x-ray energies, the scattering probability has a sharp maximum for small-angle scattering (see Fig. 5), which then produces on top of the actual interference pattern a strong intensity maximum in the direction pointing from the emitter to a nearby scatterer. Thus, this *forward focusing* effect produces maxima in directions which correspond to the emitter-neighbor bond axes and, thereby, provides direct information about the local geometry around the emitter site.[18]

The method is called x-ray photoelectron diffraction (XPD) and was successfully applied to many systems including noble metals,[19] adsorbed and self-assembled molecular layers,[20–23] ultrathin films[24] and the like (for more details see Refs. 25–27
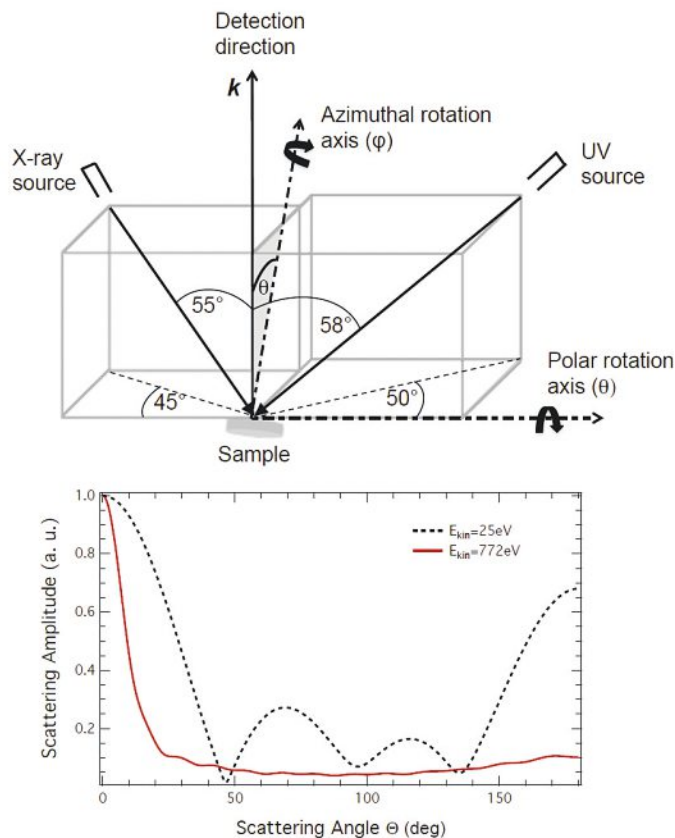
and references therein). Single-scattering codes like SSC (Single-Scattering Cluster calculations[28]) proved to be sufficient for interpreting many of these diffraction patterns, while more advanced multiple scattering codes often provide better results and even reproduce subtle details.[29,30]

The direct information provided by the forward scattering signals makes time-resolved XPD a particularly attractive tool for recording molecular movies of structural dynamics at surfaces. An x-ray probe pulse can produce a forward projected photoemission image of the molecular structure at variable time delays after the pump excitation pulse, complementary to ultrafast electron diffraction.[31] Using molecular mechanics to produce time dependent cluster coordinates for SSC calculations such a movie was simulated for CO molecules on a Pt(111) surface, which were resonantly excited by a THzpump pulse.[32,33] Since XPD experiments measure over a macroscopic surface area, the trajectories of hundreds of CO molecules were combined for ensemble averaging. As a result the thermal motion of the molecules at room temperature averages to a mean orientation which shows up as a diffraction maximum in the direction of the CO-bond axis. After the pump pulse the collective motion is reflected in the periodic and damped oscillation of the diffraction maximum in the time-resolved data.

Adsorbed molecular layers cannot be pumped too strongly in order to avoid desorption. In view of such time-resolved XPD experiments we therefore tested the sensitivity to only partial excitation of a small fraction of the molecules present on the surface mimicking real experimental conditions. We used azobenzene molecules which undergo a configurational change from trans to

cis configuration when exposed to visible or ultraviolet light. We could show that the shift of the photostationary equilibrium with light exposure could be observed in XPD.[34] In comparison with multiple-scattering calculations, the number of molecules which underwent isomerization could be estimated to about 8%. These experiments thus demonstrated the sensitivity of XPD experiments in a situation where a relatively small fraction of adsorbed molecules is involved in structural changes, thus suggesting that time-resolved XPD experiments of this kind should be feasible.

An example for XPD from an adsorbed molecular layer is shown in Fig. 6: emission from the Sn $3d_{5/2}$ core level which is well localized in the center of a phthalocyanine molecule results in the pattern in Fig. 6(f) which is displayed in stereographic projection with the radial coordinate being $\propto \tan \theta/2$, where θ is the polar emission angle with respect to the surface normal. The pattern is clearly different from that of the substrate (Fig. 6(e)). We may impose the 3-fold symmetry of the substrate in order to improve the contrast as shown in Fig. 6(g). Moreover the direct comparison with the substrate pattern and the calculation allows us to determine the orientation of the molecules, which have their mirror axis rotated by 15° relative to the densely packed atomic rows of the Ag(111) surface (Fig. 6(h)). This latter informaiton is not easily accessible by conventional electron diffraction methods.
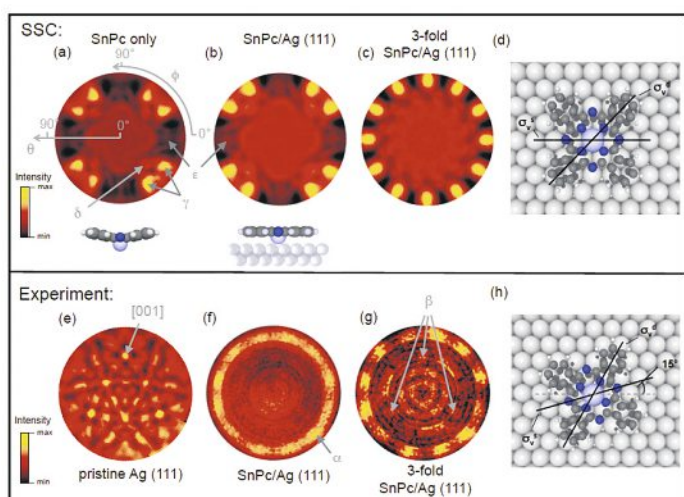

Fig. 6: XPD from a monolayer of Sn-phthalocyanine (Sn-Pc) on Ag(111) using the Sn $3d_{5/2}$ core level as emitter: SSC calculations of XPD patterns for the (a) free (and slightly bent) molecule, (b) the adsorbed molecule, (c) and three rotational domains of adsorbed molecules. Several features which change upon adsorption are indicated by grey arrows. (d) shows the molecular geometry used for the calculation. Bottom row: (e) XPD pattern from the substrate (Ag $3d_{3/2}$) which shows the typical pattern of a fcc (111)-surface; (f) Sn $3d_{5/2}$ after subtraction of a structureless background which is measured simultaneously at slightly higher kinetic energy; (g) as in (f) with imposed 3-fold symmetry of the substrate. (h) Final adsorption geometry determined by comparing the orientation of the measured and simulated patterns in (c) and (g). (Taken from ref. 15.)

Pulsed x-ray sources are scarce and currently limited to a few x-ray free-electron lasers and some exceptional high-harmonic generation (HHG) light sources.[35,36] In contrast HHG light sources in the VUV region have become readily available in many labs.[13,37–39] Therefore, we have explored the amount of structural information that can be gained from photoelectron diffraction experiments in this excitation regime, that often provides only access to valence states and not to core levels. Due to the dispersion of itinerant valence states, the intensity must here be integrated over the full bandwidth as was first shown in ultraviolet photoelectron

diffraction (UPD) experiments on Cu(111).[40] If several bands of different symmetry are crossing the signals must be disentangled before integration. Moreover, due to enhanced large-angle scattering at low kinetic energies (see Fig. 5), the strong forward focusing maxima are missing and interference effects appear more strongly. As a consequence the data are less straightforward to interpret and require more advanced simulations for quantitative analysis.[41] It was shown, however, that the method still provides information about the structural environment of the emitting state, in particular in the case of non-dispersing molecular states.[42]
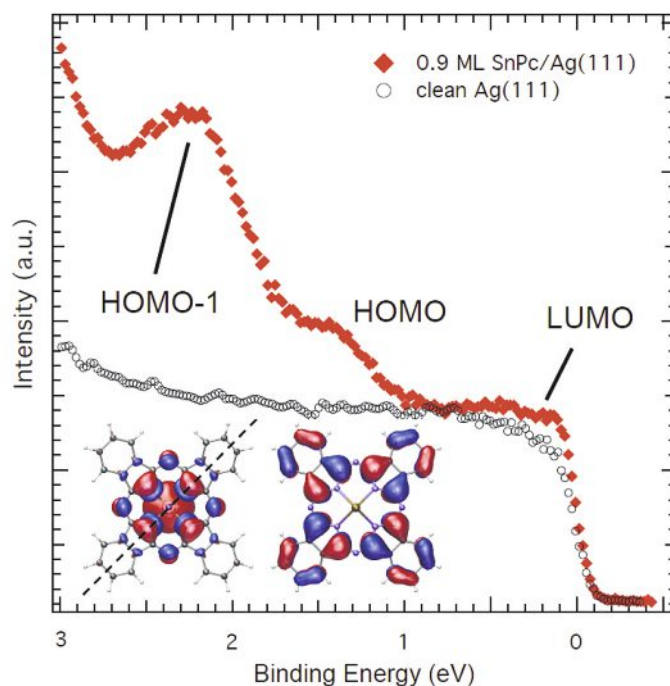

Fig. 7: Valence band spectrum (red curve) taken from SnPc/Ag(111) using VUV photons ($h\nu$= 21.2 eV), shown together with the spectrum of clean Ag(111) (black curve). The two molecular states HOMO and HOMO-1 are indicated together with the corresponding wavefunctions. The LUMO is partially occupied due to the formation of chemical bonds with charge transfer from the substrate to the molecule. (Taken from ref. 15.)

In Fig. 7 we show the valence band spectrum of SnPc/ Ag(111) taken with a helium discharge lamp and photons of 21.2 eV energy. Two prominent peaks are observed beside the onset of the partially occupied LUMO.[15] These two peaks are assigned to HOMO and HOMO-1. The latter is strongly localized at the central Sn atom and serves as emitter for the UPD measurement shown in Fig. 8(b). SSC calculations for this excitation energy were carried out using the adsorbate geometry obtained from the XPD measurements (Fig. 6). They agree reasonably well with the experimental data, considering further that the latter contain also contributions from the underlying Ag(111) substrate, as can be easily recognized when considering the measurement from the clean substrate at the same binding energy (Fig. 8(a)). Three sharp maxima show up close to normal emission in both, calculations and experiment. Their 3-fold symmetry and their absence in the calculation for the free molecule suggest that these maxima are caused by interference with electron waves back scattered at the 3-fold symmetric substrate surface. Indeed, the variation of the adsorption height of the molecule above the surface layer in the SSC calculations leads to a variation in polar angle of these three maxima. Thus, fitting the simulated positions in order to match the experimental pattern allows the height to be determined with sub-Ångström precision.[15]
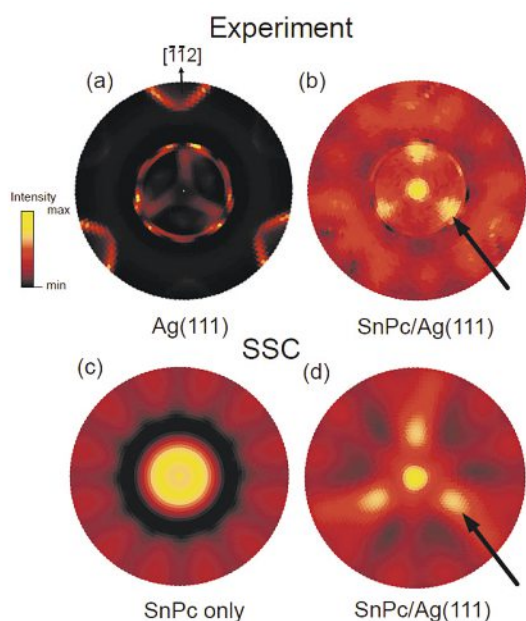
Fig. 8: UPD pattern from the HOMO-1 state of SnPc/Ag(111) recorded with photons of 21.2 eV. (a) Constant energy surface taken from the pristine substrate at the same kinetic energy. (b) Experimental UPD pattern. (c) and (d) SSC calculations for the free and the adsorbed molecule: three intense maxima which appear in simulations and experiment are highlighted by arrows. (Adapted from ref. 15.)
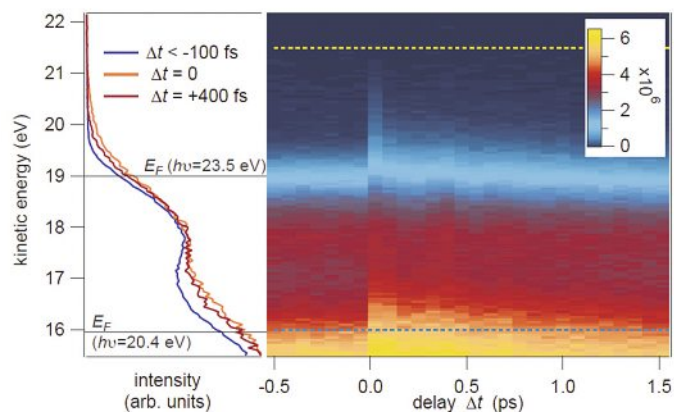

Fig. 9: Time-resolved ARPES in normal emission from the Bi(111) valence bands using two harmonics at 20.4 and 23.5 eV. Left panel: spectra at some selected time delays after the infrared pump pulse. Right panel: false-color plot of the photoemission intensity as function of energy and time delay. Note the slight periodic intensity modulation. (Taken from ref. 43.)

As proof-of-principle experiment for time-resolved UPD, we have chosen Bi(111), because the excitation with an short infrared pump pulse leads to strong displacement of the electronic charge density and to the impulsive excitation of coherent A_{1g} phonons.[44] These phonons show up as strong modulations of the energy and intensity of valence states in time-resolved photoemission spectra.[45,46] We observe such oscillatory modulations in delay scans of valence band spectra taken with VUV photons as shown in Fig. 9.[43] Interestingly the phase of the modulation depends on the momentum we are looking at as can be seen in Fig. 10: the intensity modulation at the X-point is shifted by about half a period with respect to that at the Γ-point (normal emission). This highlights one of the main differences between core-level XPD and valence level UPD experiments: the latter contain structural

and purely electronic information through the momentum-resolved density of states measured by the experiment.[43] At the X-point, the electronic structure has a large gap at the Fermi energy which means that any photoelectrons observed there are excited by indirect transitions involving phonons. In these processes they lose their memory on the initial excitation within the electronic band structure and therefore any dispersion related intensity modulation. Thus, without energy integration, their intensity modulation can be attributed to photoelectron diffraction effects.
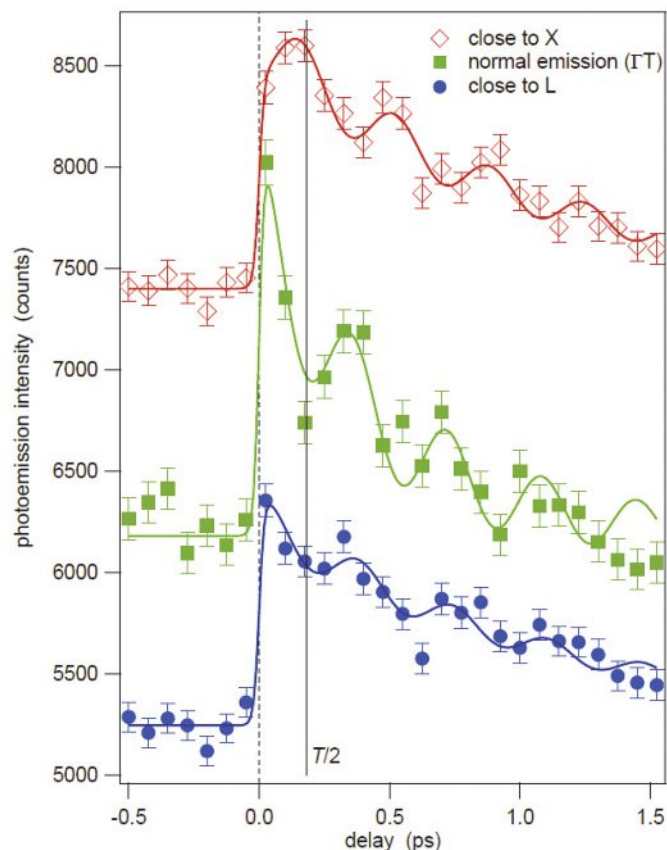

Fig. 10: Transients of the photoemission intensity taken at the Fermi energy E_F at three high-symmetry points of the Brillouin zone. The modulation of the transient from the X-point appears to be shifted in phase with respect to the other two. (Taken from ref. 43.)

Assuming a localized Bi 6p valence state we performed SSC calculations for the equilibrium and for the distorted crystal structure in order to identify spots in momentum space where the modulation of the diffraction intensity is expected to be strong. The results are displayed in Fig. 11 together with transients taken such a point (marked by the arrow in Fig. 11b). As we can see the intensity modulations at these points is identical to that found earlier at the X-point confirming our hypothesis that the transient represents the modulation of the lattice structure. Hence, within a single experiment we measure the electron dynamics and the structural dynamics, what gives us the unique possibility of determining the phase lag between the modulation of the atomic structure and the concomitant modulation of the electronic density of states.[43]

Orbital Tomography

As explained in the preceding section, interference of the outgoing electron waves generates a pattern in the final state of the photoemission process. The full final state may thus be written as a coherent superposition of direct emission and scattered waves.
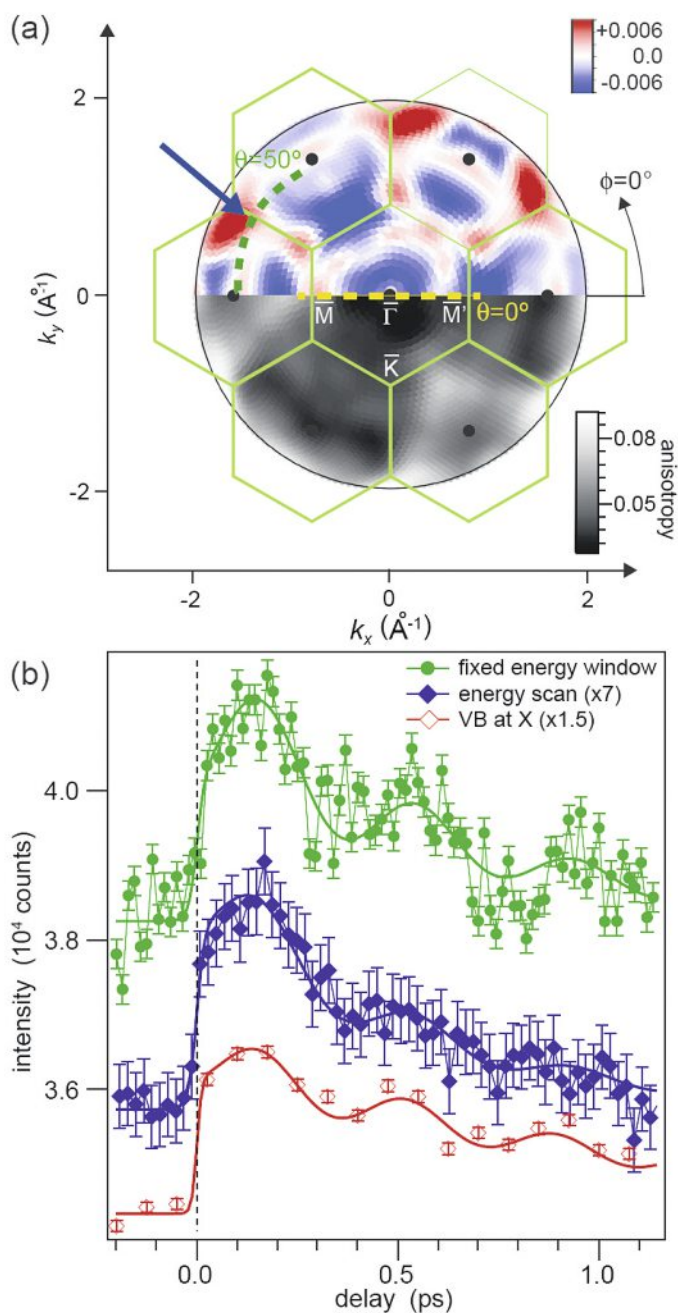
Fig. 11: (a) SSC calculation of the Bi(111) UPD using emission from a localized 6p valence state mimicking integration over the full bandwidth of the valence bands (greyscale) and the difference plot of this pattern and the corresponding pattern for the crystal distorted by the maximum amplitude of the A_{1g} mode. Red and blue colors point to maximum positive and negative differences in the diffraction pattern, respectively. (b) Transients taken at the position indicated by the arrow in the top panel and compared to the transient from the X-point in Fig. 10 (Taken from ref. 43.)

matrix element:[47] According to Fermi's golden rule an for a given photon energy $h\nu = E_f - E_i$ the photoemission rate into a direction $\vec{k}$ is proportional to the matrix element squared of the optical excitation. Assuming that final state scattering is negligible we can approximate the final state wavefunction by a single plane wave at wavevector $\vec{k}$ (for a detailed discussion of this assumption the reader is referred to Refs. 48, 49). With $\vec{A}$ being the vector potential of the incident light wave and, thus, defining the polarization vector, the square of the matrix element can be rewritten as:[47, 50]

$$
\begin{aligned}
&\left| \left\langle \psi_f(\vec{k}, E_f) \left| \vec{A} \cdot \hat{p} \right| \psi_i(\vec{k}, E_i) \right\rangle \right|^2 \\
&\propto \left| \vec{A} \cdot \vec{k} \right|^2 \left| \left\langle \exp\left(i\vec{k} \cdot \vec{r}\right) \left| \psi_i(\vec{k}, E_i) \right\rangle \right|^2 \\
&= \left| \vec{A} \cdot \vec{k} \right|^2 \left| \mathcal{F}\left(\psi_i(\vec{k}, E_i)\right) \right|^2
\end{aligned}
\tag{2}
$$

where the last line refers to the Fourier transform $\mathcal{F}$ of the initial state wavefunction. Put in other words, the angular intensity distribution represents the squared modulus of the Fourier transform of the emitter orbital. For constant photon energy and kinetic energy, the photoelectron momentum vector moves on a spherical plane with the radius being given by the photoelectron momentum inside the sample. Therefore, tuning the photon energy allows one to take spherical cuts at different radii and to obtain the full 3D Fourier transform of the initial-state wavefunction. For this reason, this method usually is referred to as orbital tomography. In pioneering experiments, Puschnig and collaborators recorded and calculated such ARPES data from delocalized occupied states in well-ordered molecular layers on metal substrates:[47, 48, 50] The projection of the ARPES data according to Eqn. 1 onto the two momentum components parallel to the surface was termed a photoelectron momentum map (PMM). The experimental PMMs are compared to simulated patterns obtained by density-functional calculations of the molecular states followed by a Fourier transform into momentum space.[47]
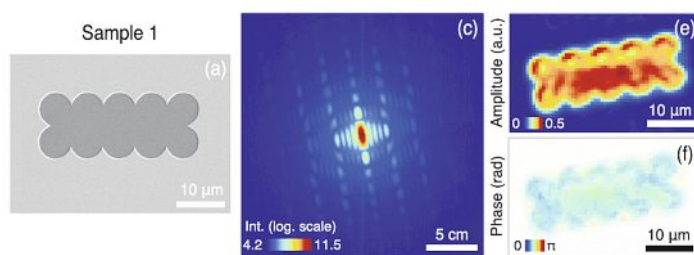

Fig. 12: Optical diffraction experiment mimicking plane-wave emission from a pentacene π-orbital. (a) Scattering target produced by lithography with the same shape than the orbital; (c) diffraction pattern of a laser beam taken behind the target. The ratio of wavelength to object size was the same for the optical experiment as for photoemission using 50 eV photons and (f) show the amplitude and phase distribution in the plane of the target, respectively, both reconstructed using a phase-retrieval algorithm. (Taken from ref. 51.)

The direct inverse Fourier transform of the PMM into real space is not possible because the experiment only provides the intensity while the phase is lost. In principle, the missing phase information can be obtained from the dichroism in measurements carried out with different circular light polarizations.[52] An alternative solution is provided by optics in the case that such data are not available: Indeed, Kliuiev *et al.* showed that the angular pattern recorded in an ARPES experiment is equivalent to the diffrac-

For light elements such as carbon, however, the scattering cross-sections are small and multiple scattering further reduces the experimental anisotropies in the VUV-range. Moreover, for delocalized initial states like π-states in organic molecules, interference effects due to backscattering from the substrate as observed in the case of the localized HOMO-1 in Sn-Pc[15] are averaged over the spatial extent of the initial state wavefunction and are thus greatly reduced. Nevertheless, a well-defined pattern with large variations in intensity is observed when looking at angular distributions from such delocalized molecular states. These patterns were shown to be the results of the angular dependence of the excitation

tion pattern produced by an electromagnetic plane wave which is diffracted off from an object of the same shape as the initial state orbital.[51] The authors then used phase-retrieval methods known from coherent diffraction in order to obtain phase information by an iterative algorithm.
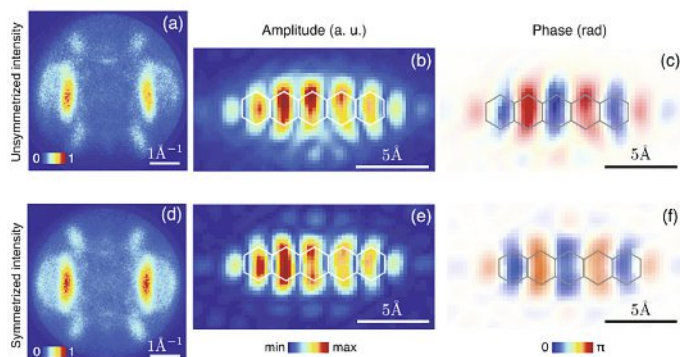

Fig. 13: Reconstruction of the pentacene LUMO from ARPES data (a) using phase-retrieval algorithms: The wavefunction amplitude (b) and phase (c), where the transparency is weighted by the amplitude for the sake of visualization, were reconstructed from the raw data without any further input. (d)-(f) idem after having applied molecular point group symmetries to the raw data prior to the reconstruction in order to reduce statistical noise on the raw data. (Taken from ref. 51.)

An example for such a reconstruction of the pentacene LUMO including the phase of the wavefunction is given in Fig. 13. In principle, no additional input was needed because the size of the molecule can be initially guessed from the auto-correlation function and then iteratively computed using the so-called shrink-wrap algorithm.[51] This size parameter is used as boundary condition to accelerate convergence. It allows the wavefunction amplitude and phase outside the molecule to be set to zero at each iteration of the algorithm because the molecular states are assumed to be confined within single molecules. Depending on the number of different orientations of the molecules present on the surface as well as the knowledge of some properties of the molecules like point group symmetries, the reconstruction may be time-consuming but has the advantage of giving direct experimental access to the wavefunctions of the molecular states.[51,53]

Moreover, when investigating molecular layers, the periodicity and the size of the surface unit cell usually are obtained from LEED, while the orientation of the molecules is often inferred from steric considerations. As a complementary method and similar to XPD, the analysis of the PMMs yields the *orientation* of the molecules adsorbed on the substrate, as will be demonstrated with data taken from the ambipolar charge-transfer complex tetrathiafulvalene-dipyrazine TTF-PYZ$_2$ assembled in dense-packed monolayers and bilayers on Ag(110).[54]

The molecules form a well-ordered monolayer when deposited on Ag(110). The angular distribution exhibits two strong maxima along the crystalline [1$\bar{1}$0]-direction of the Ag substrate as shown in Fig. 14. The higher the parallel momenta at which these peaks appear, the more localized in the center they are in real space. These maxima correspond to the HOMO, which is centered at the central TTF moiety and which has donor functionality within the complex.[56] The position of the maxima gives direct information about the orientation of the molecules. In this case the long axis of the molecules is aligned with [1$\bar{1}$0] as shown in Fig. 14. Moreover, a comparison of the data with theoretical simulation allows us to determine the bending angle of the molecules, which undergo a slight structural change when absorbed on the surface.[54] A subsequent second layer grows differently with the molecules being tilted with respect to those of the first layer and including a mirror domain. The binding energy of the HOMO states cannot be distinguished in energy in the valence band spectra, but the position of the aforementioned maxima shift in angle with respect to the substrate lattice. Hence, the tilt angle for the second layer and the mirror domain can directly be read from the angular pattern.[54]

Furthermore, the PMMs provide some sort of fingerprinting used to identify molecular states because the assignment of peaks in valence band spectra to states is often ambiguous due to missing information about the hierarchy of the states. This fingerprinting is even possible if multiple orientational domains are present on the surface, like in the case of the complex macrocycle pyrphyrin with and without Co metal center[57], which is a catalyst molecule for water splitting.[58] Adsorbed on an Ag(110)-surface the molecules exhibit multiple orientational domains.[55] The valence spectrum of the cobalt containing variant taken with 35 eV photons shows five molecular states as shown in Fig. 15. The five PMMs which correspond to the valence band peaks are shown in the top raw (raw data) and second row (after background subtraction) of the panel on the right-hand-side of Fig. 15. The molecular states were computed using DFT and the corresponding PMMs were simulated from the charge densities. The results are shown in the two bottom rows. Since the prediction of exact binding energies and even the orbital order is often difficult to obtain from DFT, the comparison with the experimental PMM data allows us to unambiguously identify the peaks and binding energies of the five states observed with the computed charge densities and molecular states.[55]

Very recently, using a combination of advanced instrumentation comprising a high-repetition-rate HHG light source[38] and a new electron detection scheme[59], Wallauer et al. succeeded in taking the first time-resolved PMMs of transiently populated LUMO states. The sample was a layer of 3,4,9,10-perylene-tetracarboxylicdianhydride (PTCDA) deposited on Cu(001), which was prepared with an ultrathin surface oxide layer for decoupling the molecules from the metal substrate.[60] The experimental set-up is shown in Fig. 16. The molecules self-assemble in two orthogonal orientations on the surface. A pump pulse in resonance with the HOMO-LUMO transition populates the LUMO. Depending on the polarization of the pump light, either molecules in a particular orientation or else all molecules can be excited. The photoelectrons are then produced by the time delayed VUV probe pulse and detected as function of parallel momentum and energy. Some time-resolved PMMs of HOMO and LUMO are shown in Fig. 17 as function of pump-probe time delay. Using oblique light incidence, the HOMO-LUMO transitions can be excited for both orientations of the PTCDA molecules, as can be seen in the experimental PMMs as well as in the simulations on the right-hand-side. While the HOMO intensity appears to be constant as function of delay (initial state bleaching can usually be neglected under typical experimental conditions) the LUMO only appears after the pump pulse and then decays on the timescale of about 100 fs.[60]

The success of this experiment shows that the measurement of excited state dynamics in real time and real space is possible using ARPES techniques. We may conjecture that in future experiments this method and the possibility of finger-printing or even reconstruction of charge densities from ARPES data will be of great help in understanding the dynamics of charge and energy transfer in solid interfaces.

Outlook: Experimental Facilities

We have seen that the angular photoelectron distribution contains a wealth of valuable information which help to determine the atomic structure and electronic charge density distributions in solid surfaces. Using pump-probe techniques, both methods can
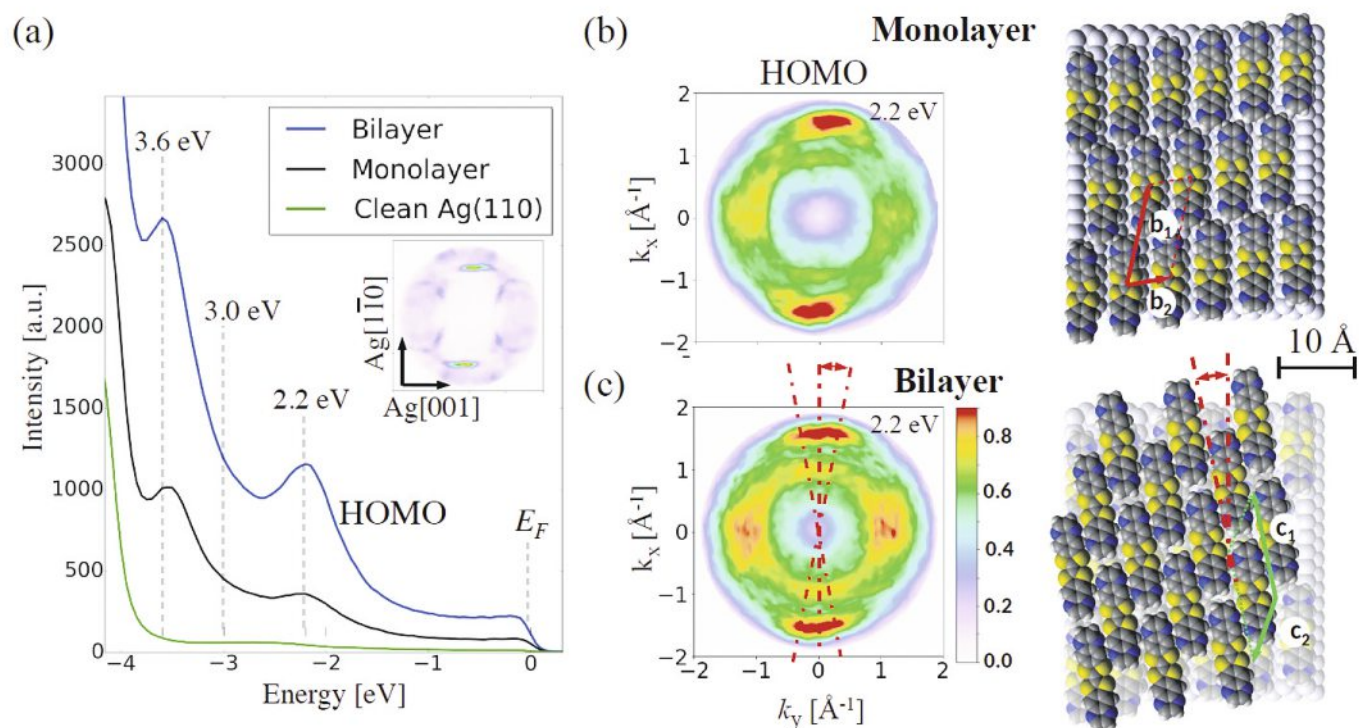
Fig. 14: Experimental acquisition of photoemission momentum maps from the HOMO of TTF-PYZ2/Ag(110) for monolayer and bilayer coverage. a) Valence band spectra taken with 21 eV photons. The HOMO appears at a binding energy of about 2.2 eV. The constant energy surface of Ag(110) taken as reference at $E - E_F$ = 2.2 eV is shown in the inset together with the orientation of the substrate. b) Angular photoelectron distribution for emission out of the HOMO for monolayer (top panel) and bilayer (bottom panel) coverage. The tilt of the molecules in the second layer is indicated by the dashed lines. c) Corresponding structural model: the blue ends correspond to the PYZ$_2$ moieties in the wings of the molecule, the central TTF part is highlighted in yellow. (Adapted from ref. 54)
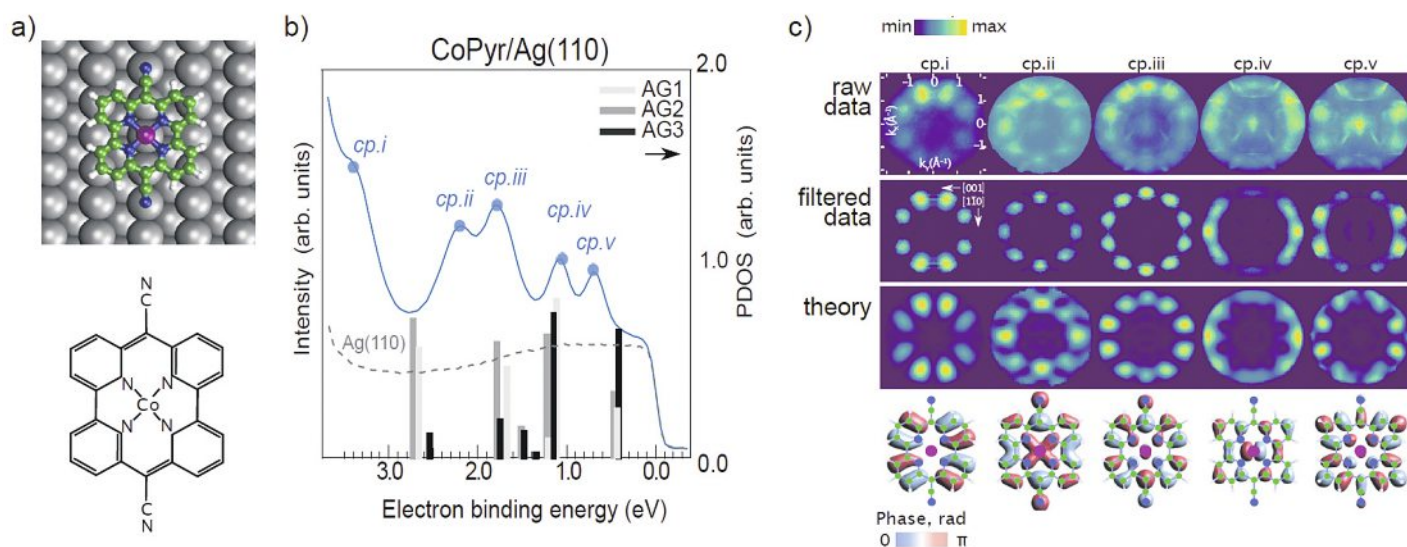

Fig. 15: Identifying molecular states in Co-pyrphyrin/Ag(110). a) Ball-and-sticks model of a molecule adsorbed with Co on top of a surface Ag atom and the long axis aligned to [1$\bar{1}$0]. b) Valence band spectrum taken with 35 eV photons and using a so-called k-PEEM detector at the NanoESCA beamline of the Elettra synchrotron; the data were integrated over the momentum range of the detector. c) Comparison of experimental and simulated tomography data showing raw data in the top raw and processed data in the center row. The data processing included the subtraction of the background signal caused by sharp Ag bands and the correction for the $|\vec{A} \cdot \vec{k}|^2$ term according to Eqn. 2. Bottom rows: simulated patterns from the molecular states summed up for three different adsorption geometries, and below, molecular orbitals derived from the DFT results and eventually assigned to the peaks (i) through (v) found in the valence band spectrum. (Adapted from ref. 55.)

be extended to real time methods with femtosecond resolution. The results together with the bandstructure and excited state lifetimes obtained from time-resolved ARPES measurements provide a complete picture of the dynamics after excitation by a pump pulse.

Such experiments take advantage of major technological developments over the past years. The number of parameters which need to be scanned for getting such a complete data set is large: The kinetic energy, two angles for the parallel momentum components, and finally the time delay require the acquisition and
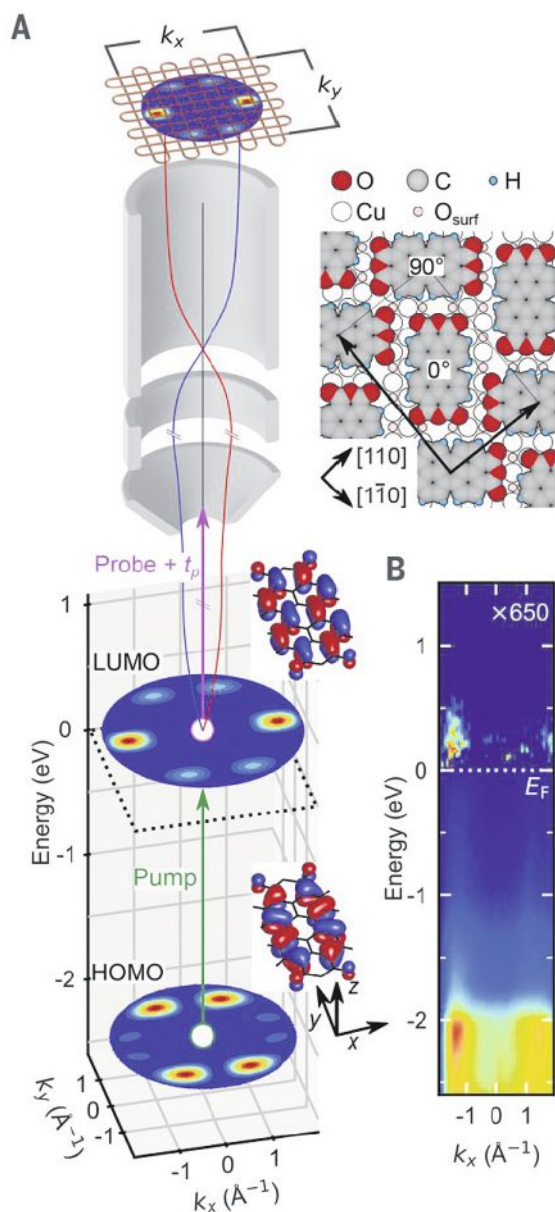
Fig. 16: Scheme of the time-resolved tomography setup: (A) Electrons are excited from the HOMO to the LUMO of PTCDA molecules by a resonant pump pulse and are probed by a VUV probe pulse and detected as function of energy and momentum. (B) Ball-and-sticks model of the molecules adsorbed in two orthogonal orientations on the surface. Bottom panel: energy distribution plotted against the momentum component kx at the instant of LUMO population. The initial LUMO population can be seen above E_F at $k_x \approx -1.5$ Å^{-1}. (From R. Wallauer et al., *Science* **2021**, *371*, 1056. Reprinted with permission from AAAS.)

analysis of at least 4-dimensional data sets. Parallel data acquisition schemes were developed resulting in so-called kPEEM momentum microscopes. They can be realized by using the Fourier image of a hemispherical photoemission microscope (PEEM) which is imaged by a second hemispherical analyzer onto a 2D detector.[61] The detector images then represent the PMM at the kinetic energy setpoint of the analyzers. A second variant uses time-of-flight technique converting electron flight time into kinetic energy. Here, the different emission angles are images by an electrostatic lens system onto the 2D delay-line detector imaged such that the image again represents the photoelectron distribution in momentum space.[62,63] The latter requires a pulsed light source owing to the flight time measurement but has the advantage of recording energy and the full parallel momentum vector at each

single shot. One of the main drawbacks of such instruments is the large space-charge which appears at intermediate focii of the imaging system with pulsed light sources. The inelastically scattered low-energy secondary electrons do not contribute to the actual signal but contain most of the photoelectrons and produce image distortions and energy shifts. One possibility to overcome this problem is the introduction of a retarding lens at the entrance of the analyzer repelling the secondary electrons close to the vacuum energy cut-off, which was demonstrated recently.[64]
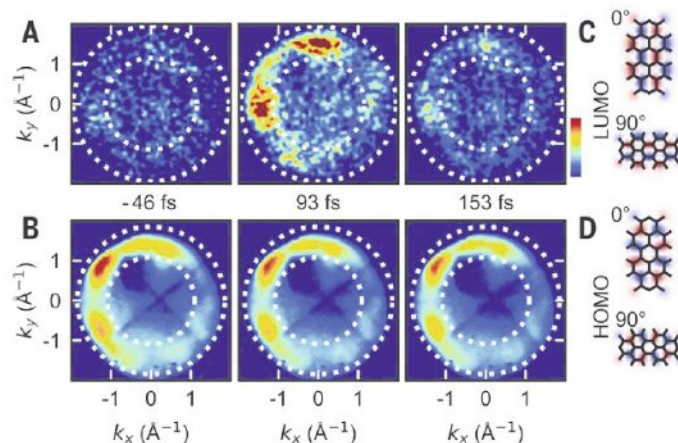

Fig. 17: Temporal evolution of LUMO (A) and HOMO (B) angular distributions for three selected time delays of the probe pulse with respect to the pump pulse, together with simulations of the patterns for the two different molecular orientations plotted in (C) and (D). While the HOMO population does not depend on the time delay, the LUMO is populated by the pump pulse at delay zero and decays on the timescale of about 100 fs. (From R. Wallauer et al., Science **2021**, *371*, 1056. Reprinted with permission from AAAS.)

On the other hand, pulsed light sources based on high-harmonic generation of VUV pulses by intense femtosecond infrared pulses in noble gas jets proved to be an excellent source for time-resolved ARPES experiments.[13, 37]

With the advent of high-repetition rate femtosecond laser amplifiers, ARPES experiments from solids at photon energies of 20 to 100 eV with repetition rates in the 100 kHz range were demonstrated by several groups.[38, 39] On top of that, many efforts were made to extend the photon energy range of laboratory experiments up to the so-called water window between the carbon K absorption edge at about 290 eV and the oxygen K-edge at about 530 eV, because this range is particularly well suited for the study of organic molecules.[35, 36] Such sources might be used for time-resolved photoelectron diffraction experiments at soft x-ray energies. Moreover, there are user facilities with dedicated ARPES endstations like the Artemis beamline at the Central Laser Facility in UK[65], the TRex facility at Elettra Sinchrotrone (IT)[66] or Harmonium at LACUS at EPFL.[67] All are HHG sources with photon energies up to about 100 eV and repetition rates of several kilo-Hertz, which are prerequisite for minimizing space-charge problems while providing high signal strength in ARPES experiments. With the advent of free-electron lasers, the range of available photon energies was extended into the soft to hard x-rays but the repetition rates are usually too low (about 100 Hz) for photoemission experiments from solids. A notable exception well suited for time-resolved ARPES is given at FLASH (DESY) with up to 4000 pulses per second,[68] a beamline equipped with a momentum microscope,[69] and a beamline with THz undulator radiation available as pump.[70] In the near future, the upgrade of the free electron laser LCLS-II of the Stanford National Ac-

celerator Laboratory includes a tremendous increase in repetition rate to about 1 MHz,[71] and a dedicated ARPES endstation will be designed in view of time-resolved photoelectron diffraction experiments at LCLS-II.[72]

Such experimental stations together with small spot sizes and flexible pump scheme extending into the THz-range for resonant pumping of low-energy modes on one side, and into the UV range for investigation of wide-band gap materials will open new possibilities for studying all kinds of solid materials with unprecedented resolution in space and time.

[1] Wikimedia, Wolfgang Pauli. 2021; https://en.wikiquote.org/wiki/Wolfgang_Pauli.
[2] Barth, J. V.; Costantini, G.; Kern, K., *Nature* **2005**, *437*, 671, https://doi.org/10.1038/nature04166.
[3] Castiglioni, L.; Greif, M.; Leuenberger, D.; Roth, S.; Osterwalder, J.; Hengsberger, M., *Chimia* **2011**, *65*, 342, https://doi.org/10.2533/chimia.2011.342.
[4] Novotny, Z.; Aegerter, D.; Comini, N.; Tobler, B.; Artiglia, L.; Maier, U.; Moehl, T.; Fabbri, E.; Huthwelker, T.; Schmidt, T. J.; Ammann, M.; van Bokhoven, J. A.; Raabe, J.; Osterwalder, J., *Rev. Sci. Instrum.* **2020**, *91*, 023103, https://doi.org/10.1063/1.5128600.
[5] Li, C.; Mishchenko, A.; Pobelov, I.; Wandlowski, T., *Chimia* **2010**, *64*, 383, https://doi.org/10.2533/chimia.2010.383.
[6] Hüfner, S. 'Photoelectron Spectroscopy: Principles and Applications; Springer Series in Solid-State Sciences', *Springer Berlin Heidelberg*, **2013**.
[7] Voit, J.; Perfetti, L.; Zwick, F.; Berger, H.; Margaritondo, G.; Grüner, G.; Hochst, H.; Grioni, M., *Science* **2000**, *290*, 501, https://doi.org/10.1126/science.290.5491.501.
[8] Koralek, J. D.; Douglas, J. F.; Plumb, N. C.; Griffith, J. D.; Cundiff, S. T.; Kapteyn, H. C.; Murnane, M. M.; Dessau, D. S., *Rev. Sci. Instrum.* **2007**, *78*, 053905, https://doi.org/10.1063/1.2722413.
[9] Yeh, J.; Lindau, I. 'Atomic subshell photoionization cross sections and asymmetry parameters: 1 ≤ Z ≤ 103', *At. Data Nucl. Data Tables* **1985**, *32*, 1–155, https://doi.org/10.1016/0092-640X(85)90016-6.
[10] Bauer, M.; Aeschlimann, M., *J. Electron Spectrosc. Relat. Phenom.* **2002**, *124*, 225, https://doi.org/10.1016/S0368-2048(02)00056-7.
[11] Grad, L.; Novotny, Z.; Hengsberger, M.; Osterwalder, J., *Sci. Rep.* **2020**, *10*, 10686, https://doi.org/10.1038/s41598-020-67589-z.
[12] Ricca, C.; Grad, L.; Hengsberger, M.; Osterwalder, J. u.; Aschauer, U., *Phys. Rev. Research* **2021**, *3*, 043219, https://doi.org/10.1103/PhysRevResearch.3.043219.
[13] Rohwer, T.; Hellmann, S.; Wiesenmayer, M.; Sohrt, C.; Stange, A.; Slomski, B.; Carr, A.; Liu, Y.; Avila, L. M.; Kalläne, M.; Mathias, S.; Kipp, L.; Rossnagel, K.; Bauer, M., *Nature* **2011**, *471*, 490, https://doi.org/10.1038/nature09829.
[14] Greif, M.; Castiglioni, L.; Becker-Koch, D.; Osterwalder, J.; Hengsberger, M., *J. Electron Spectrosc. Relat. Phenom.* **2014**, *197*, 30, https://doi.org/10.1016/j.elspec.2014.08.007.
[15] Greif, M.; Castiglioni, L.; Seitsonen, A. P.; Roth, S.; Osterwalder, J.; Hengsberger, M., *Phys. Rev. B* **2013**, *87*, 085429, https://doi.org/10.1103/PhysRevB.87.085429.
[16] Petersson, L. G.; Kono, S.; Hall, N. F. T.; Fadley, C. S.; Pendry, J. B., *Phys. Rev. Lett.* **1979**, *42*, 1545, https://doi.org/10.1103/PhysRevLett.42.1545.
[17] Thevuthasan, S.; Herman, G. S.; Kaduwela, A. P.; Saiki, R. S.; Kim, Y. J.; Niemczura, W.; Burger, M.; Fadley, C. S., *Phys. Rev. Lett.* **1991**, *67*, 469, https://doi.org/10.1103/PhysRevLett.67.469.
[18] Pillo, T.; Hayoz, J.; Schwaller, P.; Berger, H.; Aebi, P.; Schlapbach, L., *Appl. Phys. Lett.* **1999**, *75*, 1550, https://doi.org/10.1063/1.124751.
[19] Naumović, D.; Stuck, A.; Greber, T.; Osterwalder, J.; Schlapbach, L., *Phys. Rev. B* **1993**, *47*, 7462, https://doi.org/10.1103/PhysRevB.47.7462.
[20] Saiki, R. S.; Herman, G. S.; Yamada, M.; Osterwalder, J.; Fadley, C. S., *Phys. Rev. Lett.* **1989**, *63*, 283, https://doi.org/10.1103/PhysRevLett.63.283.
[21] Fasel, R.; Aebi, P.; Agostino, R. G.; Naumovi ifmmode acute c else c fi, D.; Osterwalder, J.; Santaniello, A.; Schlapbach, L., *Phys. Rev. Lett.* **1996**, *76*, 4733, https://doi.org/10.1103/PhysRevLett.76.4733.
[22] Greber, T.; Wider, J.; Wetli, E.; Osterwalder, J., *Phys. Rev. Lett.* **1998**, *81*, 1654, https://doi.org/10.1103/PhysRevLett.81.1654.
[23] Greber, T.; Šljivančanin, Z.; Schillinger, R.; Wider, J.; Hammer, B., *Phys. Rev. Lett.* **2006**, *96*, 056103, https://doi.org/10.1103/PhysRevLett.96.056103.
[24] Auwärter, W.; Kreutz, T. J.; Greber, T.; Osterwalder, J., *Surf. Sci.* **1999**, *429*, 229, https://doi.org/10.1016/S0039-6028(99)00381-7.
[25] Fadley, C. S. et al., *Surf. Rev. and Lett.* **1997**, *04*, 421, https://doi.org/10.1142/S0218625X97000420.
[26] Osterwalder, J.; Tamai, A.; Auwarter, W.; Allan, M. P.; Greber, T., *Chimia* **2006**, *60*, 795, https://doi.org/10.2533/chimia.2006.795.
[27] Osterwalder, J. *Surf. Interface Sci.*; John Wiley & Sons, Ltd, **2014**; Chapter 3.2, pp 151–214,
[28] Friedman, D. J.; Fadley, C. S., *J. Electron Spectrosc. Relat. Phenom.* **1990**, *51*, 689, https://doi.org/10.1016/0368-2048(90)80191-C.
[29] García de Abajo, F. J.; Van Hove, M. A.; Fadley, C. S., *Phys. Rev. B* **2001**, *63*, 075404, https://doi.org/10.1103/PhysRevB.63.075404.
[30] Despont, L.; Naumović, D.; Clerc, F.; Koitzsch, C.; Garnier, M. G.; Garcia de Abajo, F. J.; Van Hove, M. A.; Aebi, P., *Surf. Sci.* **2006**, *600*, 380, https://doi.org/10.1016/j.susc.2005.10.038.
[31] Carbone, F.; Hengsberger, M.; Castiglioni, L.; Osterwalder, J., *Struct. Dyn.* **2017**, *4*, 061504, https://doi.org/10.1063/1.4995541.
[32] Greif, M.; Nagy, T.; Soloviov, M.; Castiglioni, L.; Hengsberger, M.; Meuwly, M.; Osterwalder, J., *Struct. Dyn.* **2015**, *2*, 035102, https://doi.org/10.1063/1.4922611.
[33] Greif, M.; Nagy, T.; Soloviov, M.; Castiglioni, L.; Hengsberger, M.; Meuwly, M.; Osterwalder, J., *Struct. Dyn.* **2016**, *3*, 059901, https://doi.org/10.1063/1.4958888.
[34] Schuler, A.; Greif, M.; Seitsonen, A. P.; Mette, G.; Castiglioni, L.; Osterwalder, J.; Hengsberger, M., *Struct. Dyn.* **2017**, *4*, 015101, https://doi.org/10.1063/1.4975594.
[35] Tenio, P. et al., *Science* **2012**, *336*, 1287, https://doi.org/10.1126/science.1218497.
[36] Pupeikis, J.; Chevreuil, P. A.; Bigler, N.; Gallmann, L.; Phillips, C. R.; Keller, U., *Optica* **2020**, *7*, 168, https://doi.org/10.1364/OPTICA.379846.
[37] Mathias, S. et al., *Nature Comm.* **2016**, *7*, 12902, https://doi.org/10.1038/ncomms12902.
[38] Heyl, C. M.; Güdde, J.; L'Huillier, A.; Höfer, U., *J. Phys. B: At., Mol. Opt. Phys.* **2012**, *45*, 074020, https://doi.org/10.1088/0953-4075/45/7/074020.
[39] Puppin, M.; Deng, Y.; Prochnow, O.; Ahrens, J.; Binhammer, T.; Morgner, U.; Krenz, M.; Wolf, M.; Ernstorfer, R. '500 kHz OPCPA delivering tunable sub-20 fs pulses with 15 W average power based on an allytterbium laser. *Opt. Express* **2015**, *23*, 1491, https://doi.org/10.1364/OE.23.001491.
[40] Osterwalder, J.; Greber, T.; Aebi, P.; Fasel, R.; Schlapbach, L., *Phys. Rev. B* **1996**, *53*, 10209, https://doi.org/10.1103/PhysRevB.53.10209.
[41] Krüger, P.; Da Pieve, F.; Osterwalder, J., *Phys. Rev. B* **2011**, *83*, 115437, https://doi.org/10.1103/PhysRevB.83.115437.
[42] Muntwiler, M.; Auwärter, W.; Seitsonen, A. P.; Osterwalder, J.; Greber, T. 'Rocking-motion-induced charging of C$_{60}$ on h-BN/Ni(111). *Phys. Rev. B* **2005**, *71*, 121402, https://doi.org/10.1103/PhysRevB.71.121402.
[43] Greif, M.; Kasmi, L.; Castiglioni, L.; Lucchini, M.; Gallmann, L.; Keller, U.; Osterwalder, J.; Hengsberger, M. 'Access to phases of coherent phonon excitations by femtosecond ultraviolet photoelectron diffraction', *Phys. Rev. B* **2016**, *94*, 054309, https://doi.org/10.1103/PhysRevB.94.054309.
[44] Cheng, T. K.; Brorson, S. D.; Kazeroonian, A. S.; Moodera, J. S.; Dresselhaus, G.; Dresselhaus, M. S.; Ippen, E. P., *Appl. Phys. Lett.* **1990**, *57*, 1004, https://doi.org/10.1063/1.104090.
[45] Papalazarou, E.; Faure, J.; Mauchain, J.; Marsi, M.; Taleb-Ibrahimi, A.; Reshetnyak, I.; van Roekeghem, A.; Timrov, I.; Vast, N.; Arnaud, B.; Perfetti, L., *Phys. Rev. Lett.* **2012**, *108*, 256808, https://doi.org/10.1103/PhysRevLett.108.256808.
[46] Leuenberger, D.; Yanagisawa, H.; Roth, S.; Dil, J. H.; Wells, J. W.; Hofmann, P.; Osterwalder, J.; Hengsberger, M., *Phys. Rev. Lett.* **2013**, *110*, 136806, https://doi.org/10.1103/PhysRevLett.110.136806.
[47] Puschnig, P.; Berkebile, S.; Fleming, A. J.; Koller, G.; Emtsev, K.; Seyller, T.; Riley, J. D.; Ambrosch-Draxl, C.; Netzer, F. P.; Ramsey, M. G., *Science* **2009**, *326*, 702, https://doi.org/10.1126/science.1176105.
[48] Dauth, M.; Wiessner, M.; Feyer, V.; Schöll, A.; Puschnig, P.; Reinert, F.; Kümmel, S., *New J. Phys.* **2014**, *16*, 103005, https://doi.org/10.1088/1367-2630/16/10/103005.
[49] Bradshaw, A. M.; Woodruff, D. P. 'Molecular orbital tomography for adsorbed molecules: is a correct description of the fi-

nal state really unimportant?', *New J. Phys.* **2015**, *17*, 013033, https://doi.org/10.1088/1367-2630/17/1/013033.

[50] Lüftner, D.; Ules, T.; Reinisch, E. M.; Koller, G.; Soubatch, S.; Tautz, F. S.; Ramsey, M. G.; Puschnig, P. ,Imaging the wave functions of adsorbed molecules', *Proc. Natl. Acad. Sci.* **2014**, *111*, 605, https://doi.org/10.1073/pnas.1315716110.

[51] Kliuiev, P.; Latychevskaia, T.; Osterwalder, J.; Hengsberger, M.; Castiglioni, L., *New J. Phys.* **2016**, *18*, 093041, https://doi.org/10.1088/1367-2630/18/9/093041.

[52] Wießner, M.; Hauschild, D.; Sauer, C.; Feyer, V.; Schöll, A.; Reinert, F., *Nat. Commun.* **2014**, *5*, 4156, https://doi.org/10.1038/ncomms5156.

[53] Kliuiev, P.; Latychevskaia, T.; Zamborlini, G.; Jugovac, M.; Metzger, C.; Grimm, M.; Sch oll, A.; Osterwalder, J. u.; Hengsberger, M.; Castiglioni, L., *Phys. Rev. B* **2018**, *98*, 085426, https://doi.org/10.1103/PhysRevB.98.085426.

[54] Kretz, P.; Waltar, K.; Geng, Y.; Metzger, C.; Graus, M.; Schöll, A.; Reinert, F.; Liu, S.-X.; Decurtins, S.; Hengsberger, M.; Osterwalder, J.; Castiglioni, L., *New J. Phys.* **2021**, *23*, 013002, https://doi.org/10.1088/1367-2630/abcace.

[55] Kliuiev, P.; Zamborlini, G.; Jugovac, M.; Gurdal, Y.; Arx, K. v.; Waltar, K.; Schnidrig, S.; Alberto, R.; Iannuzzi, M.; Feyer, V.; Hengsberger, M.; Osterwalder, J.; Castiglioni, L., *Nat. Commun.* **2019**, *10*, 5255, https://doi.org/10.1038/s41467-019-13254-7.

[56] Jia, H.-P.; Ding, J.; Ran, Y.-F.; Liu, S.-X.; Blum, C.; Petkova, I.; Hauser, A.; Decurtins, S., *Chem. - Asian J.* **2011**, *6*, 3312, https://doi.org/10.1002/asia.201100515.

[57] Ogawa, S.; Narushima, R.; Arai, Y., *J. Am. Chem. Soc.* **1984**, *106*, 5760, https://doi.org/10.1021/ja00331a074.

[58] Joliat, E.; Schnidrig, S.; Probst, B.; Bachmann, C.; Spingler, B.; Baldridge, K. K.; von Rohr, F.; Schilling, A.; Alberto, R., *Dalton Trans.* **2016**, *45*, 1737, https://doi.org/10.1039/C5DT04426J.

[59] Tusche, C.; Goslawski, P.; Kutnyakhov, D.; Ellguth, M.; Medjanik, K.; Elmers, H. J.; Chernov, S.; Wallauer, R.; Engel, D.; Jankowiak, A.; Schönhense, G., *Appl. Phys. Lett.* **2016**, *108*, 261602, https://doi.org/10.1063/1.4955015.

[60] Wallauer, R.; Raths, M.; Stallberg, K.; Münster, L.; Brandstetter, D.; Yang, X.; Güdde, J.; Puschnig, P.; Soubatch, S.; Kumpf, C.; Bocquet, F. C.; Tautz, F. S.; Höfer, U. 'Tracing orbital images on ultrafast time scales', *Science* **2021**, *371*, 1056, https://doi.org/10.1126/science.abf3286.

[61] Tusche, C.; Krasyuk, A.; Kirschner, J., *Ultramicroscopy* **2015**, *159*, 520–529, Special Issue: LEEM-PEEM 9, https://doi.org/10.1016/j.ultramic.2015.03.020.

[62] Schönhense, G.; Medjanik, K.; Tusche, C.; de Loos, M.; van der Geer, B.; Scholz, M.; Hieke, F.; Gerken, N.; Kirschner, J.; Wurth, W., *Ultramicroscopy* **2015**, *159*, 488, Special Issue: LEEM-PEEM 9, https://doi.org/10.1016/j.ultramic.2015.05.015

[63] Schönhense, G.; Elmers, H.-J., *J. Vac. Sci. Technol., A* **2022**, *40*, 020802, https://doi.org/10.1116/6.0001500.

[64] Schönhense, G.; Kutnyakhov, D.; Pressacco, F.; Heber, M.; Wind, N.; Agustsson, S. Y. ; Babenkov, S.; Vasilyev, D.; Fedchenko, O.; Chernov, S. ; Rettig, L.; Schönhense, B.; Wenthaus, L.; Brenner, G.; Dziarzhytski, S.; Palutke, S.; Mahatha, S. K. ; Schirmel, N.; Redlin, H.; Manschwetus, B.; Hartl, I.; Matveyev, Yu.; Gloskovskii, A.; Schlueter, C.; Shokeen, V.; Duerr, V.; Allison, T. K.; Beye, M.; Rossnagel, K.; Elmers, H. J.; Medjanik, K., *Rev. Sci. Instrum.* **2021**, *92*, 053703, https://doi.org/10.1063/5.0046567.

[65] Science and Technology Facilities Council (UK), Central Laser Facility: Artemis. **2022**; https://www.clf.stfc. ac.uk/Pages/Artemis.aspx.

[66] Elettra-Sincrotrone Trieste S.C.p.A. (IT), **2020**; https: //www.elettra.trieste.it/labs/t-rex.html.

[67] Ecole Polytechnique Fédérale de Lausanne, **2022**; https: //www.epfl.ch/labs/lsu/facilities/harmonics-2/.

[68] Rossbach, J.; Schneider, J. R.; Wurth, W., *Phys. Rep.* **2019**, *808*, 1, https://doi.org/10.1016/j.physrep.2019.02.002.

[69] Curcio, D. et al., *Phys. Rev. B* **2021**, *104*, L161104, https://doi.org/10.1103/PhysRevB.104.L161104.

[70] Waltar, K.; Haase, J.; Pan, R.; Golz, T.; Kliuiev, P.; Weinl, M.; Schreck, M.; Bajt, S.; Stojanovic, N.; van Bokhoven, J. A.; Hengsberger, M.; Osterwalder, J.; Castiglioni, L., *Optica* **2019**, *6*, 1431, https://doi.org/10.1364/OPTICA.6.001431.

[71] Brachmann, A.; Dunham, B.; Schmerge, J.,39th International Free Electron Laser Conference, JACoW Publishing **2019**; FRA02, doi:10.18429/JACoW-FEL2019-FRA

[72] SLAC National Accelerator Laboratory, **2015**; https://www.osti.gov/biblio/1630267.

License and Terms